

## Article

# Al-Rich Titanites from Mont Blanc Alpine Fissures: Evidence of Ti-Nb-Y-REE Mobility during Water–Rock Interactions

Michel Cathelineau \*  and Chantal Peiffert

CNRS, GeoRessources, Université de Lorraine, F-54000 Nancy, France; chantal.peiffert@univ-lorraine.fr

\* Correspondence: michel.cathelineau@univ-lorraine.fr

**Abstract:** Titanites can be excellent markers of element transfer in medium-temperature retrograde metamorphism. Euhedral titanites from several alpine fissures from Mont Blanc, particularly those of Périades and Courtes, crystallised at the end of the main quartz stage and are synchronous with the formation of green biotites and albite before chlorite formation. Micro-XRF, SEM, electron probe, and LA-ICP-MS analyses show that these titanites have a wide range of Al<sub>2</sub>O<sub>3</sub> content from 1 to 8%, are dominated by -OH versus F, and have a wide range of Nb (up to 4500 ppm), Y (up to 3000 ppm), Zr (up to 1800 ppm), and Sn (up to 1400 ppm) concentrations. The allanite from the granite, partly destabilised into epidote, is the most likely source of Nb, Y, Zr, Sn, and REE. Titanites are enriched in HREE and show variations in LREE depending on the studied sites. Like quartz, they formed at around 400 ± 20 °C, which is compatible with the formation of green biotites after the destabilisation of granite Fe-Mg silicates. This early stage of fluid circulation, synchronous with the Mont Blanc massif uplift, is therefore marked by the titanite formation at the transition between the biotite and chlorite stability fields.

**Keywords:** titanite; niobium; REE



**Citation:** Cathelineau, M.; Peiffert, C. Al-Rich Titanites from Mont Blanc Alpine Fissures: Evidence of Ti-Nb-Y-REE Mobility during Water–Rock Interactions. *Crystals* **2024**, *14*, 472. <https://doi.org/10.3390/cryst14050472>

Academic Editor: Wolfgang W. Schmahl

Received: 19 April 2024

Revised: 2 May 2024

Accepted: 15 May 2024

Published: 17 May 2024



**Copyright:** © 2024 by the authors. Licensee MDPI, Basel, Switzerland. This article is an open access article distributed under the terms and conditions of the Creative Commons Attribution (CC BY) license (<https://creativecommons.org/licenses/by/4.0/>).

## 1. Introduction

Titanite (CaTiSiO<sub>4</sub>)[O, OH, F] is a relatively ubiquitous mineral, crystallising both at the magmatic stage, at the magmatic–hydrothermal transition (pegmatites), and during metamorphism [1–4]. Titanite has also been described in several shear zone contexts (e.g., [5]). The mineral is frequently used for dating magmatic events and high-temperature water–rock interactions (skarn deposits). Hydrothermal titanite is less described than others from the point of view of genesis and crystal chemistry. As Ti is found in titanite in octahedral coordination, it is generally replaced by Fe, Al, Nb, Ta, Mg, Zr, and Sn, and to a lesser extent by V, Cr, U, and Th, while Y and REE replace Ca. Fe, Al, and F show the most significant variability in magmatic titanite structure [4]. This extensive compilation of data makes it possible to evaluate the compositional fields of titanites from magmatic (plutonic or volcanic) and high-temperature metamorphic facies (eclogite, in particular) origin. The number of detailed studies of low- to medium-temperature hydrothermal titanites, where the crystallisation conditions have been studied using independent approaches to assess pressure, temperature, and the nature of the fluids, is much smaller than that of titanites of magmatic origin ([1,6,7]). In metamorphic rocks, Al-rich titanites seem more frequent. Some of them are characterised by enrichment in Nb or V and an OH-dominated anion site (greenschist gneisses from Andros island [8]; the Salton Sea geothermal system [9]). Regarding trace element contents of titanites, abundant data concern magmatic rocks or relatively high-temperature (>600 °C) metamorphic rocks, some related to water–rock interactions such as skarn formation [10]. Data on titanites from lower temperature hydrothermal systems are scarce, except for the Salton Sea geothermal system [9].

The aim here is to describe titanites crystallised from a hydrothermal/metamorphic fluid set in motion during phases of deformation in an exhuming mountain range, the Alps,

under  $400 \pm 20$  °C, 200–300 MPa. The example chosen are alpine fissures linked to deformation near shear zones in the Mont Blanc massif around 22 Ma [11]. The physicochemical conditions of these alpine fissures are reasonably well defined thanks to previous studies of fluid inclusions and paragenesis [12–14]. Titanites are formed from fluid in open cavities and are sometimes covered with later minerals (chlorite). As they are well preserved from deformation and alteration, they constitute one of the best-preserved markers of elemental transfer during the late stages of exhumation of the outer crystalline massifs in the French Alps. Titanite from alpine fissures unfortunately lacks precise and detailed descriptions. Euhedral titanites of millimetric size from two localities (Périades and Courtes, Figure 1) were selected because they are particularly representative, well-formed and preserved. EDS chemical maps, micro-XRF, BSE-SEM electron images, and LA-ICP-MS data were obtained on the same crystals. These data make it possible to define the mobility of trace elements (Nb, Y, REE, and Zr) during hydrothermal/metamorphic fluid events during the formation of the alpine fissures.

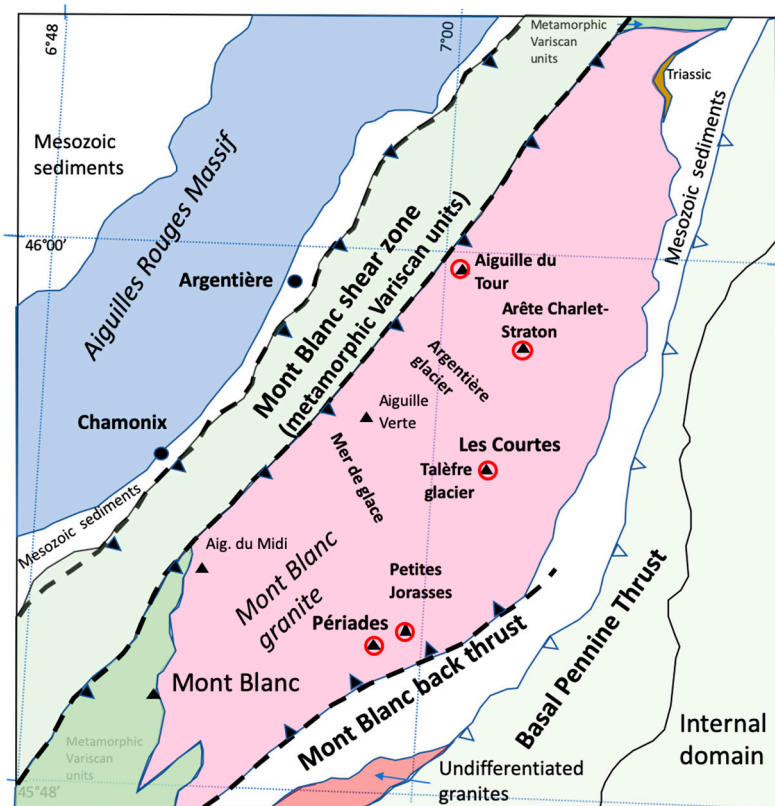


**Figure 1.** Map of the Mont Blanc massif (modified from [11]) with the locations of the studied titanites. A red circle indicates studied localities. Other triangles are important summits.

## 2. Materials and Methods

### 2.1. Local Geology

The Mont Blanc massif is one of the alpine external crystalline massifs (ECMs) that form the discontinuous belt observed at the periphery of the Alps, like that of the Aiguilles Rouges (Figure 1). The Mont Blanc massif mainly comprises a Variscan calc-alkaline granite dated  $316 \pm 19$  Ma (Rb/Sr ages, [15]). The Mont Blanc area is one of the windows in the Variscan basement beneath the Pennine and Helvetic nappes. The uplift of Mont Blanc from depths of 15 to 20 km began around 22 Ma, an age that corresponds to ages identified by the formation of newly formed biotites in the granites ( $22.8 \pm 0.6$  Ma and  $22.4 \pm 0.1$  Ma, [11]).

To the south of the massif, the Mont Blanc granite is thrust onto the Jurassic–Cretaceous sedimentary series (Figure 1). To the north, Mont Blanc is separated from the Aiguilles Rouges massif by a band of Mesozoic sedimentary rocks, commonly known as the “Cha-

monix syncline”, which outcrops in the Chamonix glacial valley. The contact zone is a shear zone (MBSz), oriented NE–SW.

During the alpine collision, the Mont Blanc granite was buried to a depth of around twenty kilometres due to the thrusting of the Valaisan domain and then the Helvetic nappes. The granite was deformed during these events, acquiring intense vertical schistosity (flattening with vertical stretching). It was metamorphosed at nearly 450 °C and 500 MPa [13,14]. The age of 29 Ma on allanite most probably indicates the age of maximum granite burial beneath the nappes [16]. Temperatures peak at 450 °C at that time and agree with estimates for the base of the Morcles nappe. In the granite, the muscovite–chlorite equilibrium in the thrust zone of the muscovite + biotite + chlorite + epidote association gives P-T estimates of  $0.5 \pm 0.05$  GPa and  $400 \pm 25$  °C, according to [13,14].

The alpine fissures formed during the thrusting of the Helvetic Nappe at around 22–20 Ma are generally close to areas of shearing and correspond to sub-horizontal tension cracks, often developed in echelon, perpendicular to the shear planes, and compatible with the SE–NW thrusting. The P-T conditions at the start of quartz crystallisation are close to  $400 \pm 20$  °C; 300–400 MPa [12,17–20]. The fractures are filled with quartz, albite, and adularia, crystallising mainly by epitaxy onto the relics of granite feldspars on both sides of the alpine fissures. The paragenetic succession is as follows: quartz Q1 (epidote), Q2-albite-adularia, chlorite, calcite-fluorite/quartz Q3-muscovite-siderite/zeolites [17].

## 2.2. Historical Works

Titanite was discovered relatively early in the Alps. Macroscopic titanite is found locally in some alpine fissures in the Mont Blanc massif. The first sample of titanite identified in France in 1780 was called “pictite” and corresponded to a prismatic form of titanite from the Mer de Glace sector. René Haüy studied a titanite crystal from Disentis near the Gotthard in 1801 and proposed calling it “sphene” in 1801 [21]. In his “Minéralogie de la France” [22], Alfred Lacroix described several specimens from the Mont Blanc massif, in particular from the area around the Talèfre glacier, and defined, among other titanite reference crystals, the following types: Type V, called the “pictite” variety, with crystals that are very elongated along the  $e^{1/2}$  edge, and Type VIII, which characterises crystals that lack elongation and flattening and are generally rich in faces (Figure 2). Since Lacroix, titanite has been found in fissures in various localities, primarily in the vicinity of Périades, along the Talèfre and Argentière basins (Les Courtes (written then in the following text “Courtes”), Aiguille du Tour, Arête Charlet Straton, and L’A. Neuve).

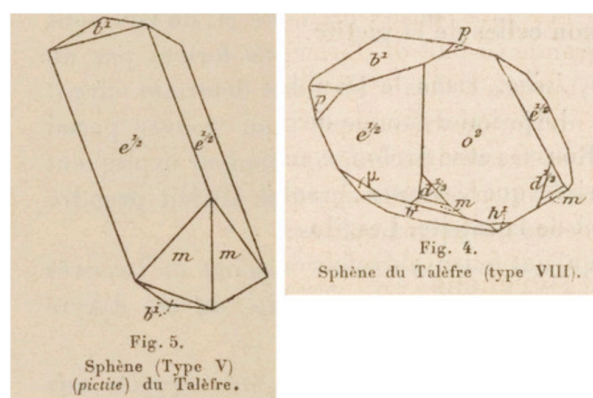


**Figure 2.** First historical drawing of titanite crystal types from the Talèfre glacier basin in 1896 (Mont Blanc massif, location in Figure 1) by [22] in his “Minéralogie de la France”.

## 2.3. Analytical Methods

Polished sections and isolated crystals were prepared and mapped in transmitted light with a Keyence VHX microscope before micro-XRF mapping on selected samples to establish the paragenetic sequence of the hydrothermal mineral assemblages.

Micro-X-ray fluorescence (XRF) mapping was carried out using a Bruker-Nano M4 Tornado instrument (SCMEM, GeoRessources laboratory, Nancy, France). This system has a Rh X-ray tube with a Be side window and polycapillary optics, giving an X-ray beam with a 25–30  $\mu\text{m}$  diameter on the sample. The X-ray tube was operated at 50 kV and 200  $\mu\text{A}$ . A 30  $\text{mm}^2$  xflash<sup>®</sup> SDD detects X-rays with an energy resolution of <135 eV at 250,000 cps. All analyses were carried out at a 2 kPa vacuum. Main elements, such as Ti, Mg, Mn, Fe, Y, Zr, and Nb, were mapped, and composite chemical images were generated. The micro-XRF mapping made choosing the most representative crystals for SEM and LA-ICP-MS investigations easier.

Scanning electron microscopy (SEM) investigations were performed on 14 samples at the SCMEM, GeoRessources laboratory (Nancy, France) using a JEOL FEG7600 apparatus 7600F (hot cathode), equipped with an Oxford Instruments SDD-type EDS spectrometer and WDS, allowing major element determination in titanite.

Electron Probe Microanalysis: A quantitative analysis of major elements was performed with a CAMECA SX100 EPMA, equipped with five WDS spectrometers, using an accelerating voltage of 15 kV, a probe current of 12 nA (an accelerating voltage of 25 kV and a probe current of 150 nA for trace elements), and a beam diameter of 1  $\mu\text{m}$ . Peak and background counting times were 10 and 5 s, respectively. The following crystals were used: TAP (F, Na, Mg, Al, Si, and Rb), LPET (K, Cl, and Nb), LIF (Mn and Fe), and PET (Cs). Standards were natural minerals and synthetic oxides: topaz (FK $\alpha$ ), albite (Na, SiK $\alpha$ ), olivine (MgK $\alpha$ ), andradite (CaK $\alpha$ ), Al<sub>2</sub>O<sub>3</sub> (AlK $\alpha$ ), orthoclase (KK $\alpha$ ), MnTiO<sub>3</sub> (Mn, TiK $\alpha$ ), Fe<sub>2</sub>O<sub>3</sub> (FeK $\alpha$ ), RbTiPO<sub>5</sub> (RbL $\alpha$ ), SrSO<sub>4</sub> (SrL $\alpha$ ), and barite (BaL $\alpha$ ).

The titanite crystals were examined with a Dilor-Labram (Horiba Jobin Yvon, France) Raman micro-spectrometer (GeoRessources laboratory, Nancy, France), using a 514.5 nm Ar<sup>+</sup> laser emission line at a resolution of 2  $\text{cm}^{-1}$  in the 100–4000  $\text{cm}^{-1}$  range. Repeated acquisition using the highest magnification was accumulated to improve the signal-to-noise ratio. Raman spectra were obtained after generally five acquisitions of 10 to 20 s each. A long working-distance objective with a 50 $\times$  magnification was used.

Titanites from alpine fissures were analysed using LA-ICP-MS (GeoRessources laboratory) to determine the trace element concentrations. Laser ablation utilised an ESI New Wave Research UC 193 nm excimer laser at a frequency of 5 Hz. The ablated material was carried by helium gas (0.5  $\text{L}\cdot\text{min}^{-1}$ ), which was mixed with argon (0.9  $\text{L}\cdot\text{min}^{-1}$ ) via a cyclone mixer (volume of 9.5  $\text{cm}^3$ ) before entering the ICP torch, and analysed with an Agilent 7900 ICP-MS. External calibration was carried out using the NIST 610 and 612 glass standards. Ti was used as an internal standard to calculate absolute concentrations. Analysed isotopes were <sup>51</sup>V, <sup>52</sup>Cr, <sup>55</sup>Mn, <sup>88</sup>Sr, <sup>89</sup>Y, <sup>93</sup>Nb, <sup>118</sup>Sn, <sup>178</sup>Hf, <sup>181</sup>Ta, <sup>182</sup>W, <sup>232</sup>Th, <sup>238</sup>U, and the REE. Data reduction was carried out using Iolite software (version 4) [23], following the standard methods from [24].

### 3. Results

The two main samples chosen from extensive works on alpine fissures are relatively large-size titanites, well formed and preserved from two localities: Périades and Courtes (Figure 3a,b). The crystals of the Périades (Figure 3c,e) are characterised by flattened crystals of a light honey colour with slightly stronger colours at the edges. Numerous inclusions of green biotite characterise the crystals from the north face of Courtes, making them opaque and dark green. Some crystals show a twinning, formed by two crystals joining together by the plane {100} (Figure 3d,f).

A few samples showing small-size titanites representative of the assemblages found at the boundary of alpine fissures (Aiguille du Tour, Les Petites Jorasses, and Arête Charlet Straton) were also studied using SEM.

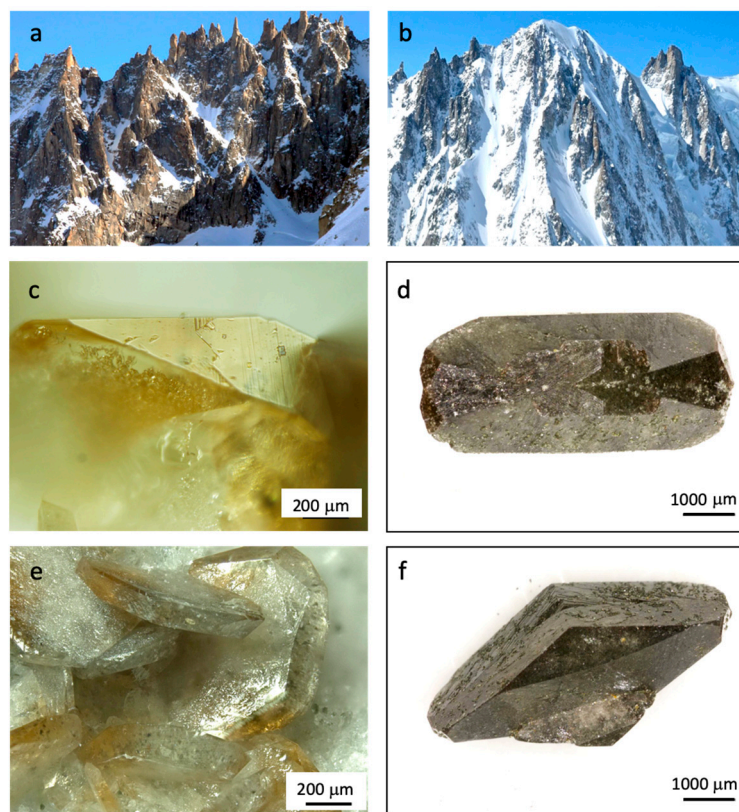


**Figure 3.** Main titanites studied and their sampling sites: (a) Périades; (b) Courtes (North face); (c,e) honey-coloured tabular titanites from Périades; (d,f) mottled titanite crystals from Courtes.

### 3.1. Petrography

From a paragenetic point of view, titanite appears late and synchronously with the late quartz overgrowth that it also overlies. Titanite is ubiquitous in the altered boundaries of alpine fissures, where it is in the form of abundant euhedral crystals no larger than 100 μm (Figure 4). A few samples were examined under SEM (Aiguille du Tour, Petites Jorasses, and Arête Charlet Straton), which show the habitus and location of these small-size titanites (Figure 4). Titanite appears associated with albite and adularia (Figure 4a,b). Euhedral apatite is in rare cases associated with titanite (Figure 4b). In Figure 4a,b, clusters of tiny euhedral crystals around 20 to 40 μm are observed, and in a few instances, larger crystals around 100 μm are found (Figure 4c). Vermicular chlorite, when present, is always located at the top of the titanite crystals and is later (Figure 4d). A careful study of the chronological relationships between titanite and chlorite, however, shows that chlorite occurs later than titanite or only appears in the last growth band of the Qtz2 quartz and titanites. Then, it crystallises abundantly on top of titanite, quartz, and albite that have already been formed (Figure 4).

When titanite is present in the cracks (examples of Périades and Courtes), the crystals are usually unmottled, shiny, and of a beautiful yellow to orange colour, sometimes intense, with sizes ranging from a few tens of micrometres to a few millimetres or even a few centimetres in exceptional cases. It crystallises on the large morion quartz Qtz2 that follows the quartz Qtz1-epidote, which is not always present.

Titanites show sectorial and locally oscillatory zonings, most frequently in the late overgrowth bands (Figure 5a–c). Biotite crystals appear as black dots due to the chosen BSE contrast in Figure 5a to reveal the titanite zoning. Biotite crystals trapped in titanite are euhedral, as shown in Figure 5b, homogeneous in mean atomic number  $Z$ , and unaltered. They appear synchronously with the titanite growth.

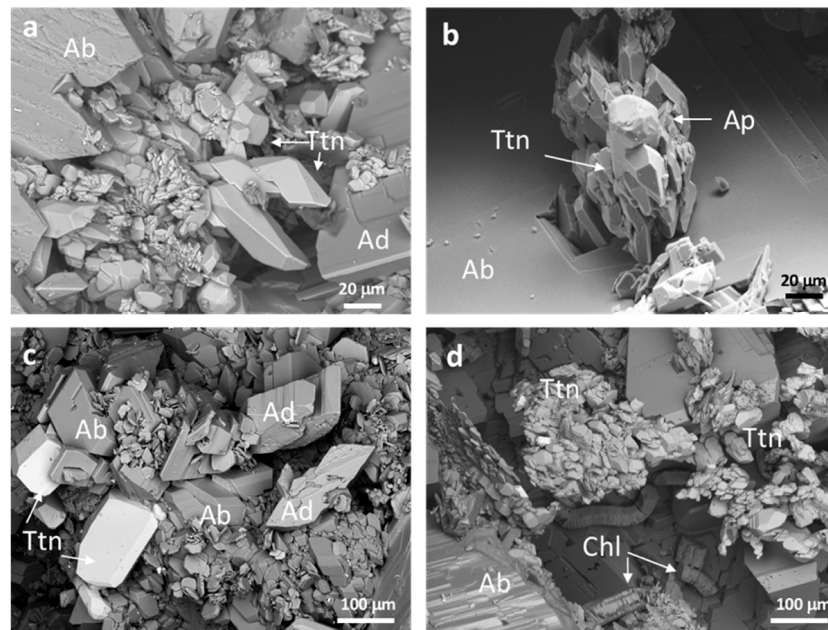


**Figure 4.** Relationships between titanite and other mineral phases in the alpine fissures of Mont Blanc (electron microscope photographs in backscattered electron (BSE) mode). (a) Titanite showing the “wedge” profile in larger crystals (40–50  $\mu\text{m}$ ) surrounded by clusters of tiny crystals on adularia and albite; (b) group of titanite spike crystals emerging from automorphic albite and topped by isogranular apatite; (c) albite-adularia association and chunky titanite crystals (in white); (d) automorphic albite and group of tiny agglomerated automorphic titanite crystals: vermicular chlorite is present in the background in the cavity in the form of “accordions” (vermicular shape) but is late. Ttn: titanite; Ab: albite; Ad: adularia; Ap: apatite; Chl: chlorite.

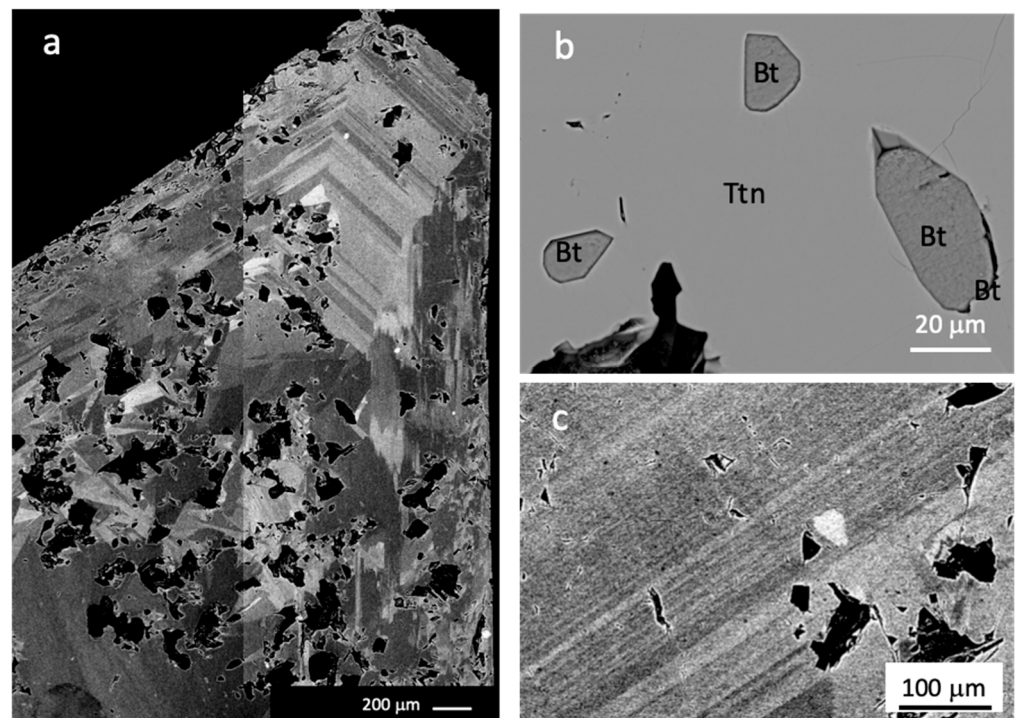


**Figure 5.** *Cont.*

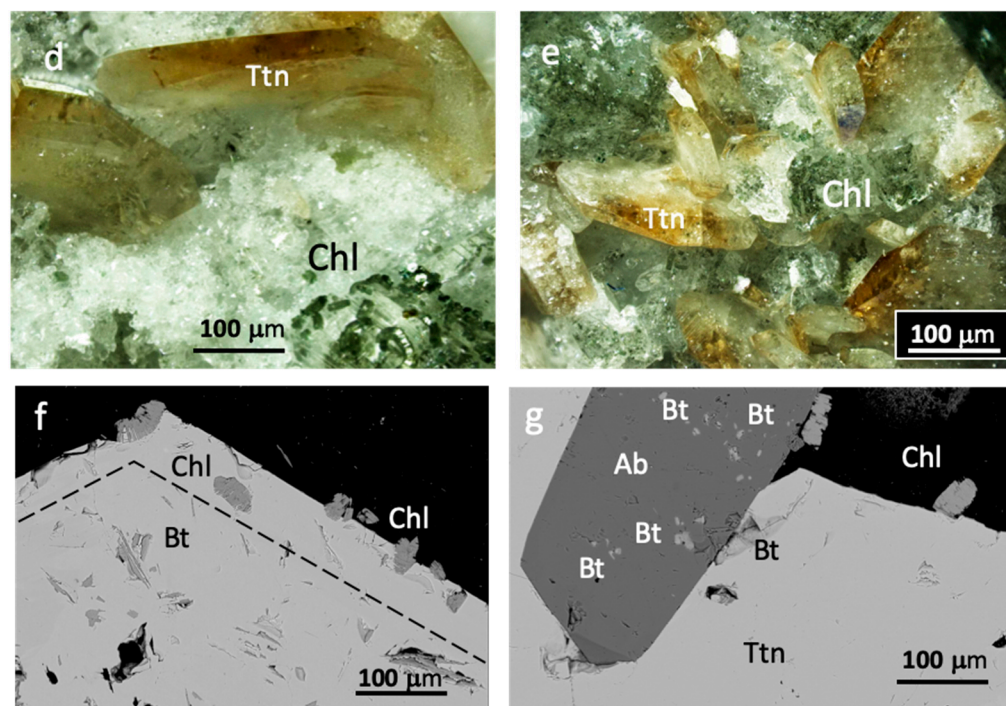


**Figure 5.** (a) BSE images of Courtes titanite showing multiple inclusions of biotites (in black) with a magnification of biotite inclusions. (b) The zoning of the external growth domain is also shown magnified in (c–e) vermicular chlorites found around titanite crystals (Périades); (f) external growth band with chlorite in and out and internal part with biotite inclusions (Courtes sample); (g) crystal from Courtes with biotite inclusions inside titanite and albite. Chlorite is found deposited onto the faces of the two minerals. Ttn: titanite; Ab: albite; Chl: chlorite; Bt: biotite.

In both localities, titanites are partially covered with vermicular chlorite, as shown in Figure 5d,e. In the Courtes titanites, an interesting transition is observed between the main crystal, where biotites form inclusions trapped during crystal growth, and the late crystal growth band, where a few vermicules of chlorites appear, the crystallisation of which ends outside titanite, and then they appear as free vermicular crystals (Figure 5f,g). This sample, therefore, represents one of the best examples illustrating the relative timing of the biotite-to-chlorite transition.

### 3.2. Crystal Chemistry Data

#### 3.2.1. Major Elements

Titanites from the Mont Blanc massif show quite contrasting levels of overall substitution of titanium by other elements (Al and Fe) (Figure 6, Table 1, and Appendix A). In Figure 6a, which contrasts the occupation of the titanium site by the different chemical elements substituting it (Fe and Al), the titanites from Périades have the lowest level of titanium substitution, followed by those from Courtes, and finally the other sites in the massif.

In the  $\text{TiO}_2$  versus  $\text{Al}_2\text{O}_3$  diagram (Figure 6b) proposed by [25], the titanites from Mont Blanc have  $\text{Al}_2\text{O}_3$  concentrations that range from 0.6% to 8% (data in Table 1). Titanites have more restricted concentrations at the scale of a crystal or a site. For example, the titanites from Périades have the lowest  $\text{Al}_2\text{O}_3$  concentrations (0.77 to 0.97%), those at Courtes have concentrations between 1.7 and 3.8%  $\text{Al}_2\text{O}_3$ , while titanites from other localities, particularly those from Aiguille du Tour, reach 7.6 to 7.9%. Aluminium is, therefore, the main substituent for titanium in Mont Blanc titanites. In Courtes titanites, the F content is low and ranges from 0.45 to 0.95%, with a mode close to 0.8%. It is positively correlated with Al and Fe. Périades titanites are fluorine-free, and have the lowest concentrations of Fe and Al.

In the Fe-Al diagram (Figure 6c), many of the titanites analysed are characterised by low iron values, unlike those at Courtes, which show an Fe/Al correlation with a ratio of 1/8 and iron atomic concentrations between 0.01 and 0.02 p.f.u.

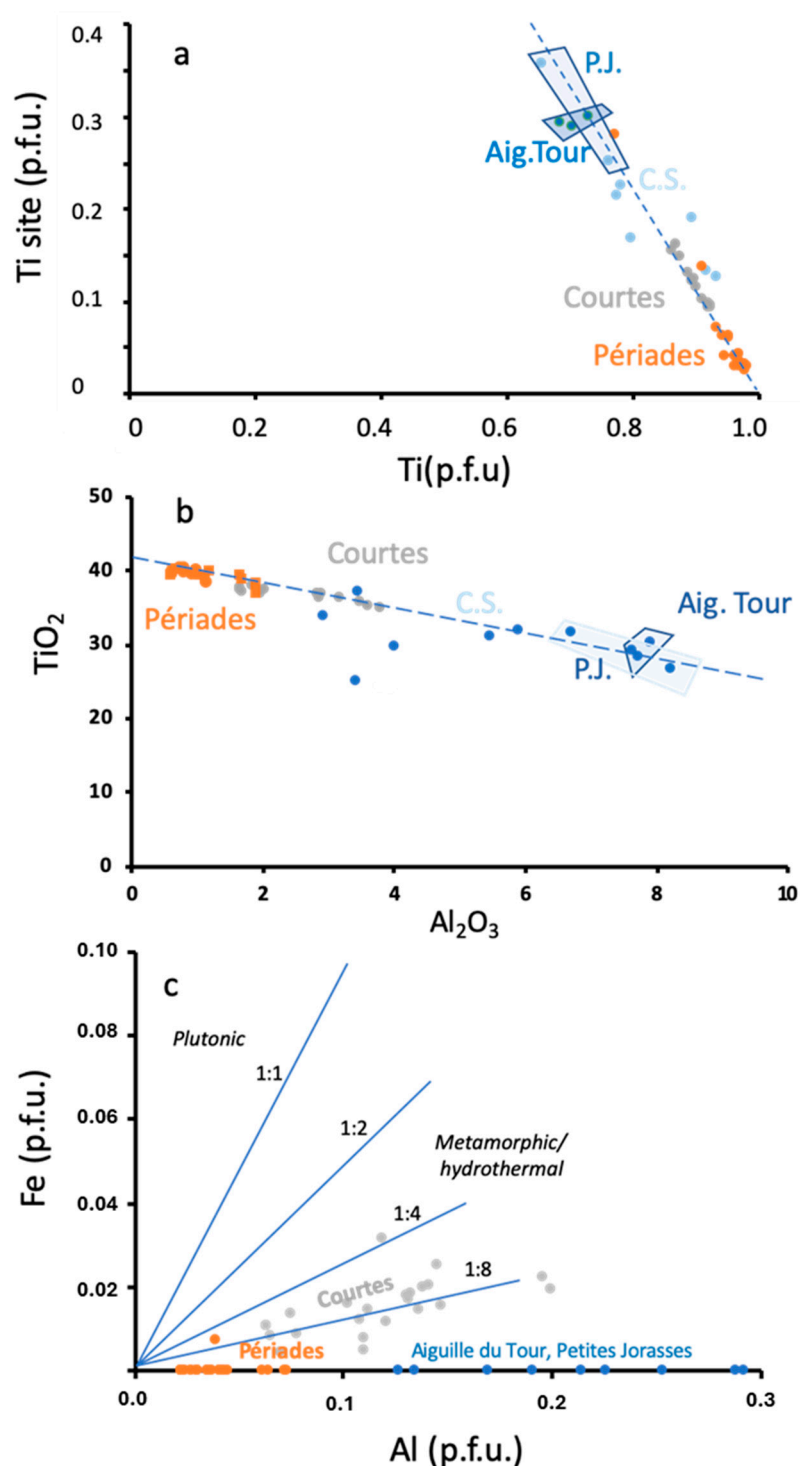


**Figure 6.** Crystal-chemical diagrams applied to Périades and Courtes titanites, and a few analyses performed on titanites from other localities (C.S.: Charlet Straton; P.J.: Petites Jorasses; Aig. Tour: Aiguille du Tour). (a) Ti site infilling by other cations than Ti versus Ti content (p.f.u.: per formula unit); (b) TiO<sub>2</sub> versus Al<sub>2</sub>O<sub>3</sub> diagram; (c) Fe versus Al diagram from [4]. The main fields for plutonic or metamorphic/hydrothermal are from [4].

**Table 1.** Representative chemical composition of titanites (oxides in wt%) and structural formulae calculated based on five oxygens. Total iron is expressed as FeO. b.d.l.: below detection limit. Charlet St: Charlet Straton; P. Jorasses: Petites Jorasses; Ag. du Tour: Aiguille du Tour. a.p.f.u.: atomic proportion per formula unit calculated.

Wt.%	Périades				Courtes				Charlet St.	P. Jorasses	Ag. du Tour
SiO <sub>2</sub>	30.11	30.31	30.17	30.19	31.27	30.71	30.61	30.49	30.96	32.97	33.32
CaO	28.34	28.05	28.26	29.65	28.86	28.67	28.86	28.32	31.10	28.66	30.46
TiO <sub>2</sub>	39.28	38.14	38.67	40.15	35.31	35.23	37.76	37.30	32.02	31.65	28.48
Al <sub>2</sub> O <sub>3</sub>	1.32	1.72	2.11	1.02	3.60	3.80	1.65	1.70	5.91	6.72	7.75
Fe <sub>2</sub> O <sub>3</sub>	0.11	0.17	0.16	0.10	0.81	0.63	0.44	0.33	0.00	0.00	0.00
Y <sub>2</sub> O <sub>3</sub>	1.29	0.78	0.89	0.00	0.00	0.00	0.00	0.00	0.00	0.00	0.00
Nb <sub>2</sub> O <sub>3</sub>	0.45	0.23	0.13	0.02	0.00	0.00	1.16	0.99	0.00	0.00	0.00
ZrO <sub>2</sub>	0.13	0.04	0.10	0.00	0.00	0.00	0.30	0.39	0.00	0.00	0.00
F	0.00	0.00	0.00	0.00	0.82	0.96	0.52	0.54	0.00	0.00	0.00
total	101.05	99.62	100.61	101.43	99.77	98.98	99.28	98.11	99.99	100.00	100.01
a.p.f.u.											
Si	0.98	1.00	0.98	0.98	1.02	1.01	0.99	1.00	1.01	1.06	1.07
Ca	0.99	0.99	0.99	1.03	1.00	1.01	1.00	1.00	1.08	0.98	1.05
Ti	0.96	0.94	0.95	0.98	0.86	0.87	0.92	0.92	0.78	0.76	0.69
Al	0.05	0.07	0.08	0.04	0.14	0.15	0.06	0.07	0.23	0.25	0.29
Fe	0.00	0.00	0.00	0.00	0.02	0.02	0.01	0.01	0.00	0.00	0.00
Y	0.02	0.01	0.02	0.00	0.00	0.00	0.00	0.00	0.00	0.00	0.00
Nb	0.01	0.00	0.00	0.00	0.00	0.00	0.02	0.01	0.00	0.00	0.00
Zr	0.00	0.00	0.00	0.00	0.00	0.00	0.00	0.01	0.00	0.00	0.00
F	0.00	0.00	0.00	0.00	0.04	0.05	0.03	0.03	0.00	0.00	0.00

### 3.2.2. Trace Elements

Two crystals from Périades exhibit interesting chemical zonings, illustrated in Figures 7 and 8. The micro-XRF mapping of the titanite crystal has revealed their chemical zonations, particularly in trace elements such as Nb, Y, and Zr.

The first crystal from Périades (Figure 7) indicates that quartz Qtz2 and albite may be incorporated within the titanite crystal during titanite growth. As shown in Figure 7b, titanite grew probably because of the aggregation of smaller crystals of microscopic size (several tens of microns), which then fuse into a single macroscopic crystal. The crystal shows sectorial zoning with some zones enriched in Y and others enriched in Nb and Zr.

In the second crystal from Périades (Figure 8a–c), a core slightly enriched in Fe (zone I) is rimmed by a zone richer in Nb and Y (Zone II). A last growth band with oscillatory zoning is revealed by means of BSE-SEM images (Figure 8d,e). This band (zone III) shows similar trace element patterns to zone II but is still enriched in most elements such as Nb (3680 ppm in zone III compared to the 1200–2700 ppm range in zone II; Table 2, graph from the bottom of Figure 8f).

**Table 2.** Representative LA-ICPMS analyses of titanite trace elements from the two mostly studied sites, Périades and Courtes (all elements in ppm).

ppm	V	Cr	Mn	Sr	Y	Zr	Nb	Sn	Hf	Ta	W	Th	U
Périades													
PER2-1	142.8	12.2	470.7	38.9	2342.1	41.9	317.2	122.3	1.96	6.35	6.28	5.1	12.7
PER2-2	145.3	12.1	398.4	36.8	2252.2	33.6	203.5	108.6	1.67	6.15	2.40	2.8	7.6
PER2-3	141.9	13.8	372.0	36.7	1570.0	20.5	118.7	86.3	1.08	4.03		1.6	4.4
PER2-4	135.9	15.2	356.1	33.3	354.2	2.3	21.2	45.6	0.00		0.34	0.2	0.7
PER2-5	140.5	15.0	353.5	34.8	353.8	3.3	29.1	51.1		0.39			0.8
PER2-6	78.5	5.9	365.1	40.5	912.5	200.4	1313.6	425.9	8.95	27.6	1.24	0.6	1.5
PER2-7	79.0	5.4	365.0	40.2	863.1	190.0	1252.3	422.1	9.22	28.8	1.57	0.6	1.4
PER2-8	83.7	6.1	379.7	40.7	967.1	196.8	1162.5	449.9	8.92	18.7	5.71	0.9	1.9

Table 2. Cont.

ppm	V	Cr	Mn	Sr	Y	Zr	Nb	Sn	Hf	Ta	W	Th	U
PER2-9	85.1	5.6	371.8	39.8	925.8	212.9	1359.0	428.5	10.59	24.4	3.04	1.0	1.8
PER2-10	84.1	5.3	367.8	41.5	904.7	243.6	1462.2	423.5	13.80	37.6	1.73	0.9	1.8
PER2-11	80.0	5.4	344.7	45.7	1434.2	740.2	2313.9	720.6	34.44	93.9	1.14	2.7	4.4
PER2-12	82.3	6.0	334.1	49.7	1563.2	967.8	2691.8	839.7	43.48	122.2	1.27	3.2	4.7
PER2-13	77.6	5.0	344.3	52.5	1495.7	1420.1	3690.7	1143.2	57.60	163.5	1.21	4.7	6.2
PER2-14	81.4	5.5	322.8	52.1	1489.1	842.6	2300.2	796.1	46.47	150.8		2.1	2.8
PER1-1	79.3	5.1	352.2	58.9	1414.1	1339.4	4506.5	1078.0	58.72	169.3	0.52	3.8	4.9
PER1-2	67.8	5.3	369.1	53.6	1735.6	1790.3	4857.6	1365.7	62.15	141.9	2.04	6.4	11.5
PER1-3	65.3	6.8	463.5	55.4	3208.8	44.6	2411.9	551.1	1.87	38.38	85.8	18.3	41.4
PER1-4	84.0	12.3	605.4	50.7	3276.9	102.5	2054.6	605.5	4.87	28.2	55.4	12.4	76.9
PER1-5	98.0	9.5	500.5	49.5	2831.4	53.3	1637.6	417.6	2.15	23.3	123.1	15.3	41.2
PER1-6	138.4	12.5	452.5	38.0	2246.6	43.9	393.1	125.8	1.89	7.40	6.50	5.1	12.9
PER1-7	151.8	9.8	377.0	37.8	1623.8	22.2	150.8	96.9	1.17	4.80	1.46	1.8	5.1
PER1-8	167.4	13.3	351.1	36.5	231.4	1.4	24.6	44.0	0.00		0.08		0.4
Courtes													
B-1	430.8	42.2	305.2	21.1	187.8	21.0	109.5	137.1	1.24	3.17	1.27		7.4
B-2	383.9	71.5	375.5	26.3	1111.4	213.8	1735.6	742.3	6.88	6.98	269.8		717.5
B-3	384.0	64.9	305.6	27.9	1279.0	38.2	1917.8	406.4	1.48	8.67	65.62	0.7	148.6
B-4	473.0	58.2	289.9	20.3	772.0	51.0	531.1	178.7	1.68	2.36	63.04		93.1
B-5	473.9	59.4	308.7	21.7	802.5	59.5	692.8	252.4	1.94	3.30	76.84	0.1	159.1
B-6	445.1	55.6	287.1	20.8	720.7	54.0	509.7	225.1	0.69	2.39	60.78		82.0
B-7	462.4	61.1	309.1	23.9	887.2	35.3	993.3	265.1		5.06	51.55	0.0	60.1
C-1	442.2	19.7	239.3	22.3	208.9	25.6	115.3	156.0	1.07	3.14	1.53		3.9
C-2	418.3	52.6	234.4	18.2	432.5	18.2	137.3	116.5		0.76	3.70	0.0	8.3
C-3	405.4	47.0	249.6	19.1	580.4	47.9	276.3	198.6	2.29	1.51	6.85		15.1
C-4	504.0	39.9	334.0	21.8	1040.3	127.5	1025.3	374.9	5.37	4.37	100.7		415.6
C-5	382.7	62.9	335.9	25.5	1032.5	97.5	1727.8	475.4	4.67	9.69	80.4	0.0	105.2
C-6	435.0	91.6	364.5	24.0	1171.4	178.2	1080.0	706.2	10.53	5.23	2907.2	0.0	144.2
C-7	399.4	68.9	305.2	23.6	909.8	169.0	920.5	606.7	8.58	3.66	2285.0		94.7

Trace element concentrations obtained through LA-ICP-MS on two profiles from Périades and two profiles from Courtes were carried out after the micro-XRF mapping. They are shown in Table 2 and Figure 9.

Nb, Zr, and Y concentrations reach thousands of ppm in some growth bands (LA-ICP-MS, confirming the X-ray microfluorescence data and the maps shown in Figures 7 and 8). Nb concentrations range from 20 to 5000 ppm, Y from 180 to 330 ppm, Zr from 1 to 1800 ppm, and Sn from 35 to 1400 ppm. Nb, Zr, and Sn are positively correlated to Y. A single profile from Périades stands out from the others in a zone of Périades titanite, for which the Y concentration is much higher than the others, covering the 1500–3300 ppm range and corresponding to the sectorial zoning enrichment shown in Figure 7d,e. Even higher Y values may be expected in this crystal, as the profile crosscuts the sector but not at the maximal mapped enrichments. The Périades titanites are enriched in most metals compared to those from Courtes, W, U, V, and Cr excepted, and correspond to the titanites with the lowest Fe and Al contents.

The sum of REE reaches ranges from 300 to 2800 ppm. In Périades titanites, the spectra normalised to the chondrites are not very fractionated and show a moderate negative Eu anomaly (Figure 10). In Courtes titanites, the REE spectrum is much more fractionated, with a relatively low LREE content and slight inflexion at the Eu level. Overall, the spectrum is fractionated in favour of HREE, which reaches values close to, but lower than those of Périades titanites by a factor of 2 (Figure 10).

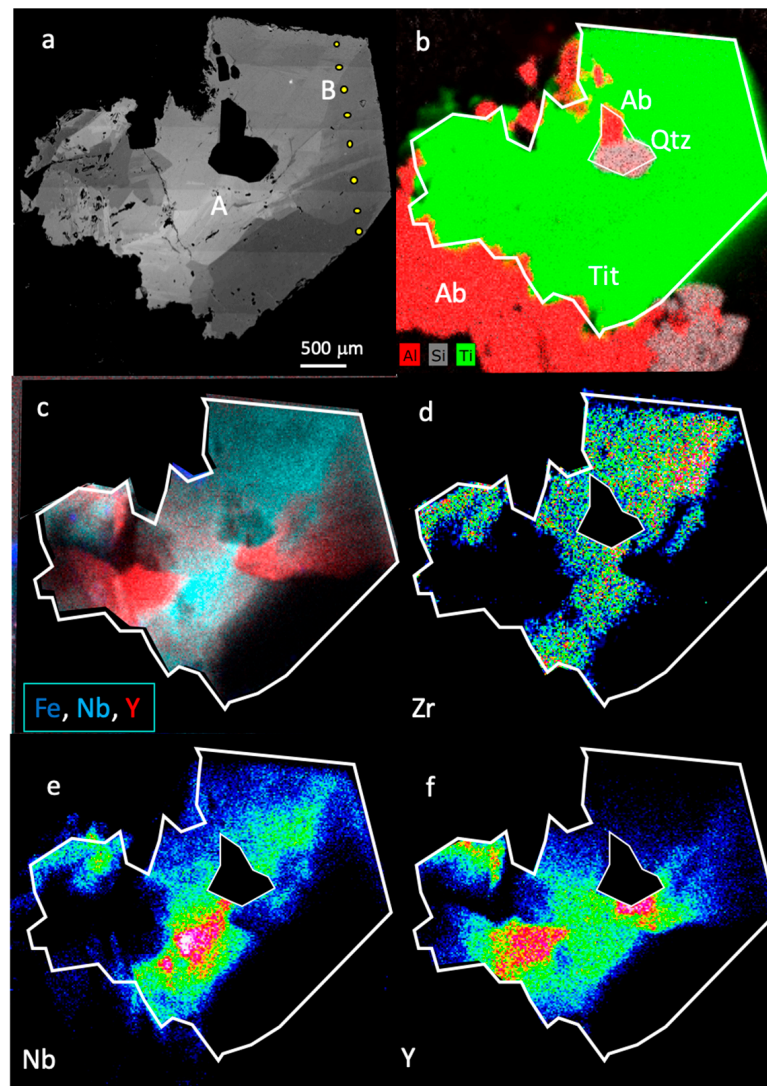


**Figure 7.** Périades titanite crystal (Per-Ti1). (a) BSE-SEM images with the indication of the LA-ICP-MS profile and Raman analyses (A, B). (b) Composite chemical image showing that titanite has grown, including small quartz and albite crystals. (c–f) micro-XRF chemical maps of the same titanite crystal (Zr, Fe, Nb, and Y composite). (d,e) BSE-SEM images of the inset indicated in (a), showing oscillatory zoning of the external growth band.

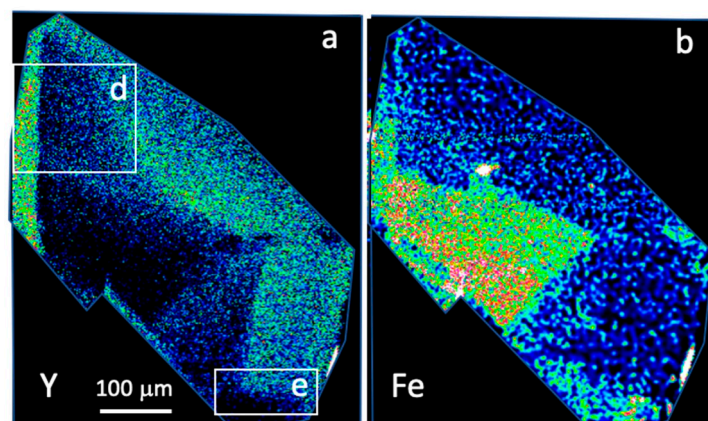


**Figure 8.** *Cont.*

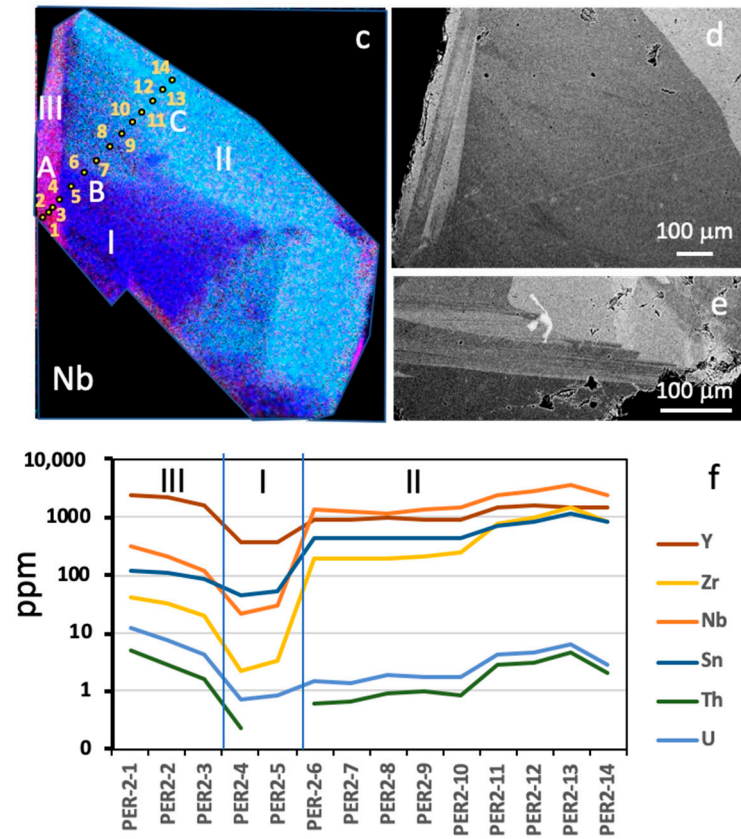


**Figure 8.** Périades titanite crystal (PER-Ti2). (a) Y; (b) Fe; (c) Nb with an indication of the LA-ICP-MS profile and Raman analyses (A, B, C). (d,e) BSE-SEM images of the inset indicated in the figure, showing oscillatory zoning in the external growth band. At the bottom of (f), the chemical profile localised in (c) is provided.

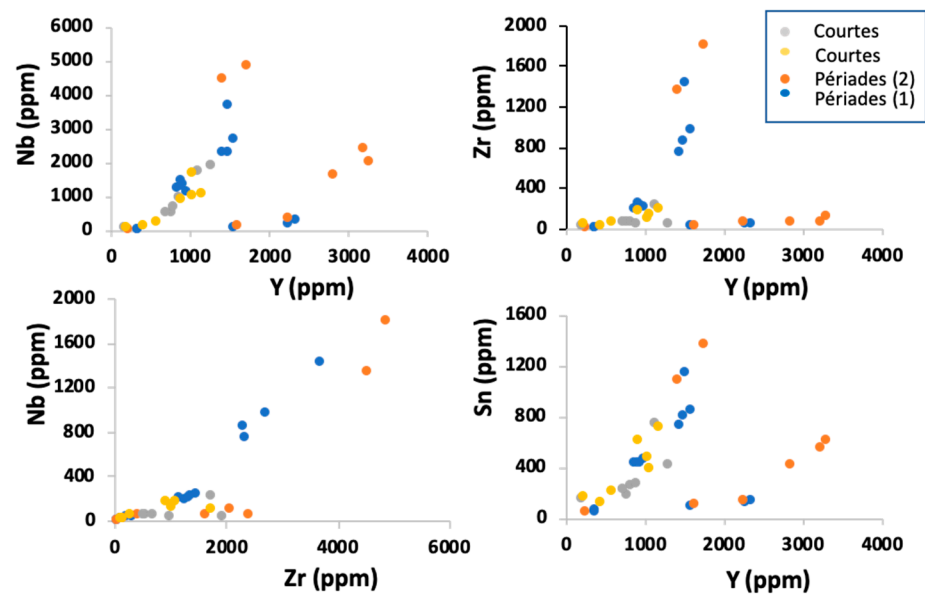


**Figure 9.** Trace elements analysed using LA-ICP-MS in titanites from Courtes (two crystals) and Périades (two profiles, one by crystals shown in Figures 5 and 6).

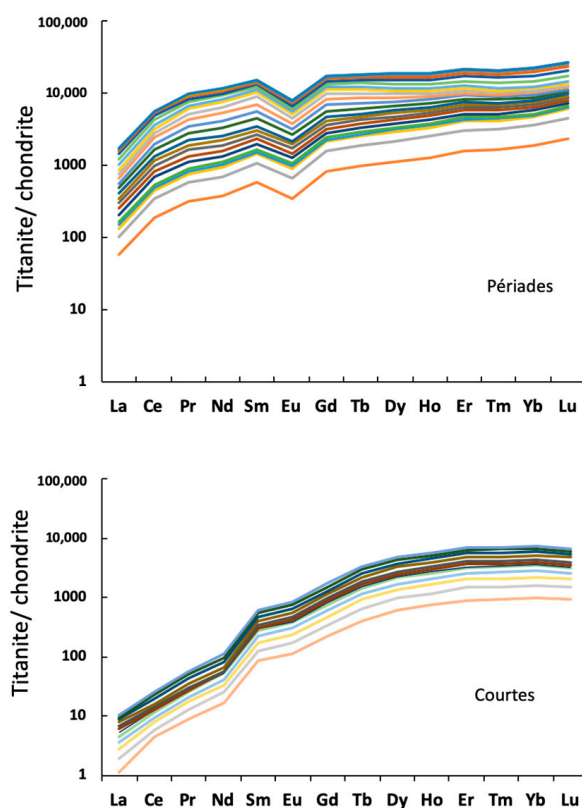


**Figure 10.** REE spectra normalised to chondrite of titanites from Périades and Courtes. The different colored lines correspond to each analysis from the mentioned profiles in Figures 7 and 8.

### 3.3. Raman Spectra

Representative Raman spectra obtained from the analysed titanite samples are shown in Figure 11 and correspond to areas characterised by contrasted trace element distribution: two Raman spectra for titanite Per-Ti1 with a zone enriched in Zr (noted A) and a zone enriched in Nb (noted B); three Raman spectra obtained on Per-Ti-2 (Figure 8 for the location), corresponding to zones enriched in Y and Fe (A), Fe (B), and Nb (C); and, finally, two representative Raman spectra of Courtes titanites which do not display any significant zoning.

All spectra exhibit characteristic peaks near 248, 333, 603, 881, 965, 1033, 1173, 1236, 1312, and 1545  $\text{cm}^{-1}$ . The main differences between spectra concern the relative intensity of some bands, particularly the two intense bands at 603 and 881  $\text{cm}^{-1}$ . Another difference concerns the bands 217–229 and 248  $\text{cm}^{-1}$ , which display similar intensities or an increased intensity of the 248  $\text{cm}^{-1}$  band.

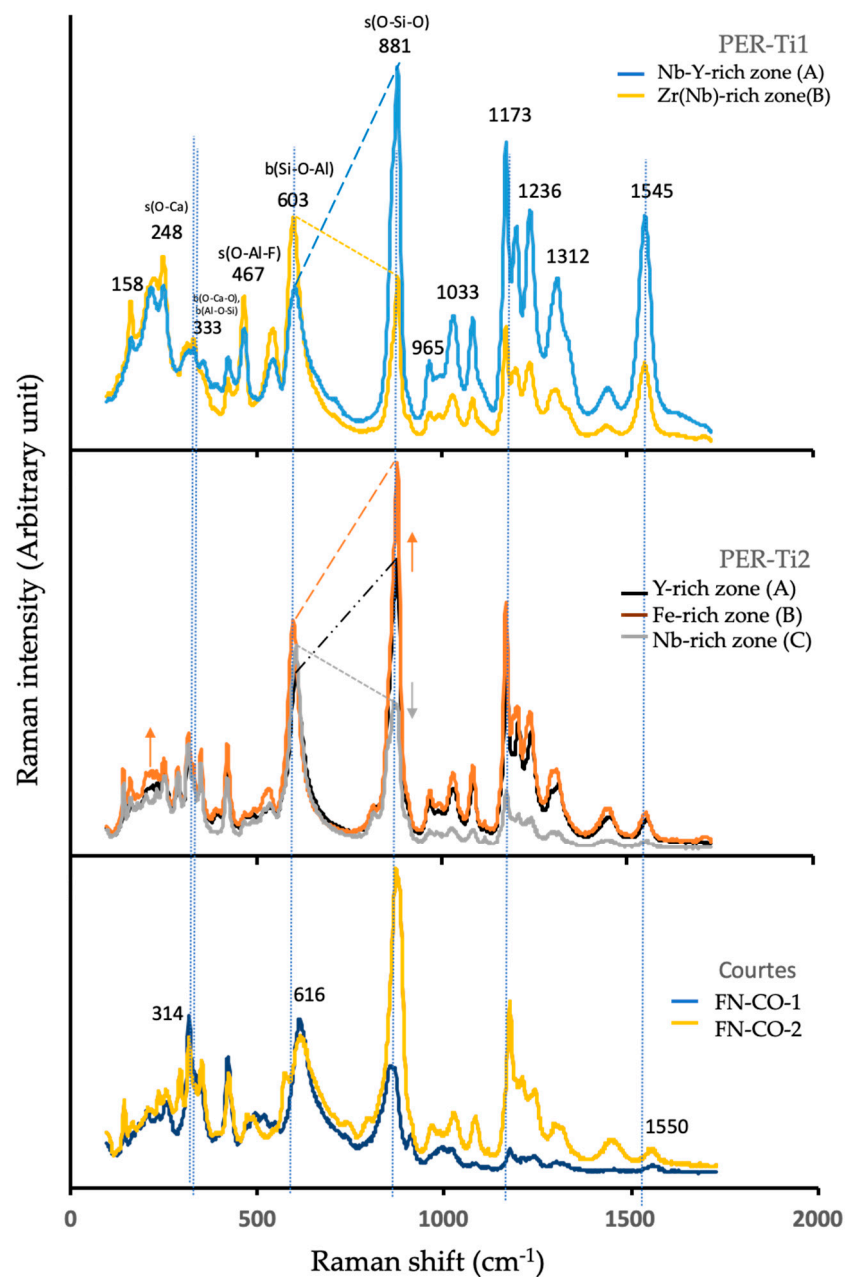


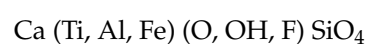
**Figure 11.** Raman spectra of Mont Blanc titanites. Périades: crystals PER-Ti1 and PER-Ti2 (location of analysed zones in Figures 7 and 8, respectively), and Courtes (two crystals, FN-CO-1 and FN-CO-2). Band assignment follows [26,27].

## 4. Discussion

### 4.1. Incorporation of Trace Elements into the Titanite Structure

Titanite is a nesosilicate in which the isolated silica tetrahedra ( $\text{SiO}_4^{4-}$ ) are bonded to cations or anionic groups and not to other silica tetrahedra. The isolated silica tetrahedra are bonded to a folded chain of  $\text{TiO}_6$  octahedra, which shares the corners and is parallel to the crystallographic axis.

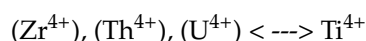
There are several possible substitutions in each site of titanite. The most common substitution of quadrivalent Ti is by trivalent Fe and Al, leading to a formula of the type:



This results in a charge imbalance generally compensated by a coupled substitution of  $F^-$  or  $OH^-$  for the oxygen (called O1), under-bonded relative to the other oxygens in the structure [25,28]. The suggested substitution to maintain the electrical equilibrium is:



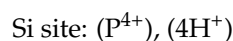
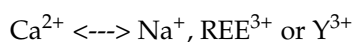
Ti site: besides  $Al^{3+}$ , titanium can also be replaced by the following elements [[8,28–30]:  $Mg^{2+}$ ,  $Fe^{2+}$ ,  $(Cr^{3+})$ ,  $(Zr^{4+})$ ,  $(V^{5+})$ ,  $Nb^{5+}$ ,  $(Ta^{5+})$ ,  $(Th^{4+})$ , and  $(U^{4+})$ . In this site, substitutions may occur at a constant charge:



Or, by the introduction of trivalent and pentavalent cations to maintain the charge balance [25,29,31]:



Ca site: calcium ions occupy relatively large cavities with unusual sevenfold coordination [30]. It can be substituted by  $Na^+$  and large cations, including  $Sr^{2+}$ ,  $Ba^{2+}$ ,  $Y$  + MREE,  $(U, Th, Mn, \text{ and } Pb)$  [32]. The introduction of monovalent and trivalent cations maintains the charge balance:



The elements written in bold are those identified in the Mount Blanc titanites in significant amounts. In the Mont Blanc titanites, Al is mainly substituted for titanium, with Fe remaining low. Compared with the reference titanites analysed by [25], the Mont Blanc titanites display an Al content which covers the entire worldwide range. The titanites have high concentrations at the crystal or site scale. The titanites of Périades are the lowest in  $Al_2O_3$  (0.77 to 0.97%), those of Courtes have between 1.7 and 3.8%  $Al_2O_3$ , while the titanites of other localities, in particular that of the Aiguille du Tour, reach 7.6 to 7.9%.

The iron content is low so that in the Fe-Al diagram of [4], the low to very low Fe/Al ratios place the Mont Blanc titanites broadly within the wide range of hydrothermal to metamorphic titanites defined by these authors but at the lowest Fe content. The very low Fe values are typical in the compiled data on eclogitic formations [4], which do not correspond to the Mont Blanc geological context. According to [4], the charge balance in metamorphic, hydrothermal, and pegmatitic titanite due to the substitution of  $Fe^{3+}$  and  $Al^{3+}$  in the  $Ti^{4+}$  site is mainly achieved by the coupled substitution of  $F^-$  for  $O^{2-}$ , which is only partially the case in Courtes and not the case in Périades. In Courtes titanites, F is correlated with Al, with a F/Al ratio of 1/3.3. As Al is trivalent and three times (in p.f.u.) more abundant than fluorine, the contribution of fluorine to the electric balance is relatively low (1/10).

#### 4.2. Raman Data

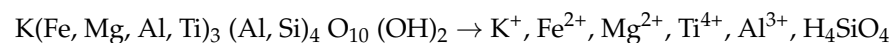
The Raman spectra of Mont Blanc titanites exhibit the same bands as those predicted using numerical modelling and those from RRUFF Pakistan titanites. Main bands are attributable by analogy to data from [26,27]: at 248–252  $cm^{-1}$  to the translational vibration of  $[SiO_4]^{4+}$ , around 580–600  $cm^{-1}$  to O-Si-O and Si-O-Al bending modes, and around 881  $cm^{-1}$  to O-Si-O symmetric stretching bonds. It is rather difficult to correlate the shift in the bands' intensities to chemical changes observed in the crystals, which mainly concern trace elements and Al-Fe content. The differences cannot be due to a different crystallographic orientation, as analyses were performed in single crystals. Therefore, the crystallographic orientation must be similar between the analysed points. However, differences in band intensities are not easily related to the changes in trace element contents.

The spectra are identical to the spectrum R050114 from RRUFF [33], which corresponds to titanite from Skardu (Roundu, Gilgit, Pakistan), e.g., alpine-cleft-type metamorphic deposits, similar to the alpine clefts. The cleft in Pakistan formed in granite and amphibolite lithologies during the tectonic deformation associated with the Main Karakoram Thrust. As in Mont Blanc, the thrust produced many fractures and clefts where alpine-type minerals developed.

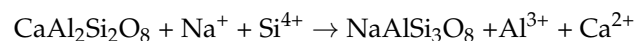
#### 4.3. Mechanism of Titanite Formation

The Ti/Al ratio of the fluid controls the composition of the titanite. These two elements are paradoxically considered relatively insoluble, particularly in aqueous fluids with a low contribution of volatiles (CO<sub>2</sub>) identified in the fluid inclusions in quartz. Al is generally regulated by equilibria with aluminosilicates, i.e., the two feldspars (albite-adularia), as shown by the Na/K ratios of alpine fluids from Mont Blanc [12,17]. Thus, the Na/K ratio of around 6.9–6.8, found either using the crush-leach technique or LIBS on fluid inclusions, indicates an equilibrium with the two alkali feldspars within the 350–400 °C range.

The Ti/Al ratio of the fluid is then controlled by the Ti concentration in the fluid, which depends on the rate of alteration of the biotites from the granite and the rate of reincorporation during the formation of the alpine green biotites. In the deformed granite, the biotite dissolves and releases K, Ti, Fe, and Mg according to the following simplified reaction:



All these alterations occur before the titanite is deposited in the presence of stable, newly formed green biotites. The temperature range is around 400–420 °C to keep the biotite stable, not below. What is original in the alpine fissure case is that titanite and green biotites are synchronous. Titanite precipitation in cavities needs calcium, which is available from the albitisation of the anorthite component of granite plagioclases. This dissolution reaction can be written with constant Al or with Al mobility:



The fluids related to quartz growth are aqueous (H<sub>2</sub>O is dominant, Cl around 1 mol%, Na (930 ± 90 mmol/kg H<sub>2</sub>O), K (135 ± 35 mmol/kg H<sub>2</sub>O) Li (30 ± 8 mmol/kg H<sub>2</sub>O), Ca (105 ± 25 mmol/kg H<sub>2</sub>O), and minimal amounts of CO<sub>2</sub> + N<sub>2</sub>). In addition, as pCO<sub>2</sub> is relatively low and subsequently carbon is present as bicarbonate in solution under a neutral pH preserving feldspars, no calcite precipitates. Calcite precipitates later in the mineral sequences of the Mont Blanc alpine clefts, probably due to a temperature decrease or fluid mixing [12,17]. The formation of Al-rich titanites with a high CaAlSiO<sub>4</sub>-OH<sup>-</sup> component seems favoured by relatively low-temperature conditions [9]. These authors described Al<sup>3+</sup>-rich metamorphic titanites in the metasediments of the Salton Sea geothermal system. There, the Al/Fe ratio of titanites decreases with increasing temperature and depth from 0.3 ± 0.1 pfu in the chlorite-calcite zone (180–320 °C) through 0.17 ± 0.05 pfu in the biotite zone (330 ± 10 °C), to 0.12 pfu in the clinopyroxene zone (350 ± 10 °C). In Mont Blanc, titanites crystallised at temperatures around 400 ± 20 °C and are also aluminous, low in iron, and dominated by OH<sup>-</sup>.

According to [9], titanites are favoured by the degradation of granite biotites, which allows titanite-Al-OH to crystallise. In Mont Blanc, Fe-Mg silicate dissolution in the bleaching zone releases some elements that are then reintegrated into the crystallisation of both titanite and green biotite (Fe, Al, and Si). The co-crystallisation of titanite and biotite is, at least in the Courtes example, perfectly demonstrated by textural studies. Let us suppose that sufficient calcium is present in the solution. In that case, titanite can reach oversaturation because the solution is sufficiently loaded with dissolved silica, as

shown by the precipitation of abundant quantities of quartz in the alpine fissures, which is synchronous with titanite (last increment of the Q2 quartz stage and small euhedral quartz trapped in titanite). A conceptual model of Ti transfer is shown in Figure 12. When calcium is less abundant, titanium oxides, such as brookite, anatase, and rutile, can form, and all three polymorphs with the formula  $TiO_2$ . However, this is not the case in the studied alpine fissures, in contrast with other alpine massifs such as Oisans, where the lithologies are very different (amphibolites) and anatase is locally abundant.

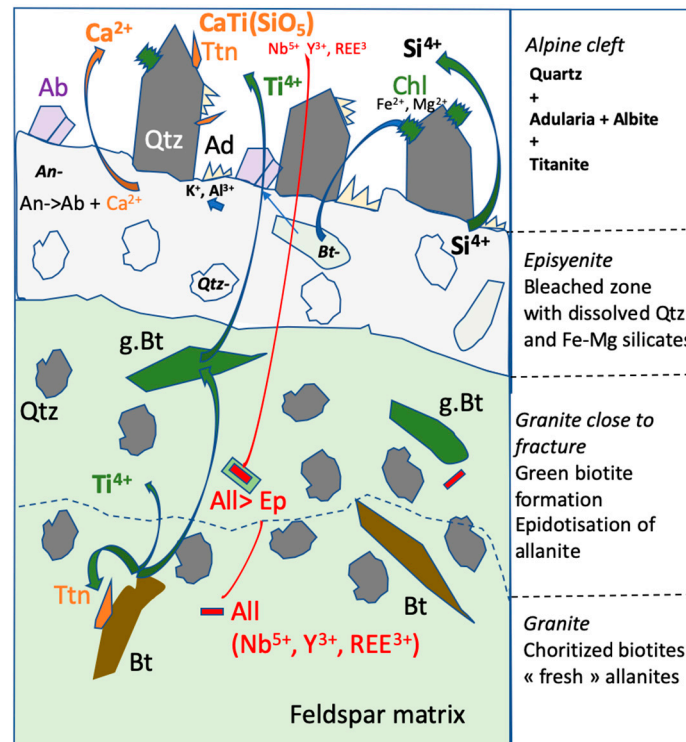


**Figure 12.** Conceptual model of titanite formation: titanium is released by the dissolution of ferro-magnesian silicates in the bleaching band (episyenite), whereas quartz is also unstable and completely dissolved. Titanites crystallise in the paragenesis Qtz2 + albite + adularia with green biotites. Trace elements (Nb, Y, and REE) are liberated both from the bleached zones and the alteration of the granite allanite and their alteration secondary mineral phases. Ab: albite; An: anorthite; Ad: adularia; Ttn: titanite; Chl: chlorite; Qtz: quartz; Bt: biotite; g. Bt: green biotite; All: allanite; Ep: epidote.

The amount of titanite precipitated (mm in size in some cavities) is very low compared to the mass of Ti released during granite bleaching, which occurs all around the cavities and along faults. If an altered rock volume of 10 cm of bleaching is considered on a meter square, the weight of released Ti (if 100% is leached) is 780 g  $TiO_2$ . Considering titanite density of 3.5 g/cm<sup>3</sup>, this weight corresponds to 222 cm<sup>3</sup> of titanite, e.g., 16,000 grains of titanites of millimetric size (2 × 1 × 1 mm), thus more than 100 hundred times the amount of observed titanite in the exceptional cases. That means that the efficiency of the reprecipitation of Ti is less than one %, and Ti is mobile in altering fluids, contrary to what is generally assumed in mass balance calculations [14]. However, some Ti released is also precipitated in green biotites with a  $TiO_2$  content between 0.8 and 1.3%.

#### 4.4. Origin of Nb, Y, and REE in Titanite

The main carrier of Nb, Y, and REE in granite is allanite, the most abundant accessory mineral. However, allanite is most often altered to epidote in the vicinity of alpine fissures, which may have resulted in the release of these elements in fluid phases. The allanite-to-epidote conversion has also been described along shear zones in the Mont

Blanc massif [14]. Allanite is the main carrier that can explain the concentrations of Nb (20–30 ppm), Y (30–45 ppm), or REE (sum around 150 ppm) in the Mont Blanc granite [14].

The differences in the REE spectra of the titanites from the two localities may be due to primary accessory source minerals in the granite having different rare-earth availability or to selective trapping by other minerals. For example, when epidote forms at the expense of allanite, it can trap some of the elements released when the allanite dissolves. Allanites being dissolved or replaced release trace elements that can be incorporated first in the epidote as an in situ alteration product of allanite and then by titanite or other phases, such as described in shear zones by [14]. The local partition between allanite and epidote or others such as Y-bearing phases such as aeschynite ((Y, Ca, Fe, Th)(Ti, Nb)<sub>2</sub>(O, OH)<sub>6</sub>), or thombartite (Y<sub>4</sub>(Si, H<sub>4</sub>)<sub>4</sub>O<sub>12-*x*</sub>(OH)<sub>4+2*x*</sub>) described by [14], may explain the local availability of REE(Y) and the differences in concentration levels in titanite. In addition, some titanites co-grow with biotite (Courtes), while others do not incorporate biotite crystals during their growth. The presence or absence of biotites may reveal differences in the characteristics of the percolating fluids, particularly whether fluids are oversaturated or not with respect to biotites. Other differences may concern their rate of disequilibrium with REE-Y-Nb source minerals.

## 5. Conclusions

- Euhedral titanites from several alpine fissures on Mont Blanc, particularly those of Périades and Courtes, provide some essential information about element transfers related to the development of alpine fissures in the Mont Blanc massif.
- Titanites crystallised at the end of the crystallisation of the principal quartz in the alpine fissures (Qtz2 stage) and are synchronous with the crystallisation of green biotites and albite, around  $400 \pm 20$  °C.
- As they predate the deposition of chlorites, titanites mark the transition between the biotite and chlorite stability domains in the Mont Blanc massif.
- The titanites are rich in Al. OH dominates the OH-F site, as fluorine remains relatively low or is absent, such as in the Courtes sample. They are thus quite different from magmatic titanites characterised by high Fe and F contents.
- Titanites show a wide range of concentrations of trace elements such as Nb, Y, Zr, Sn, and REE. Although some sectorial zoning could explain differences in the distribution of concentrations, these elements are generally positively correlated. No simple relation could be established with the titanite structure, as most Raman spectra display remarkable similarities, apart from two bands at 603 and 881 cm<sup>-1</sup> with varying intensities.
- The granite allanite, partly destabilised into epidote, is the most likely source of Nb, Y, Zr, Sn, and REE. Titanites are characterised by rare-earth spectra enriched in HREE and show variations in LREE depending on the location in the Mont Blanc massif. They are, therefore, excellent markers of element transfer in medium-temperature retrograde metamorphism for elements generally considered relatively immobile, such as Ti, Zr, and Nb.

**Author Contributions:** Conceptualisation, M.C.; methodology, M.C.; software, C.P.; investigation, M.C.; resources, M.C.; data curation, C.P.; writing—original draft preparation, M.C.; writing—review and editing, M.C.; funding acquisition, M.C. All authors have read and agreed to the published version of the manuscript.

**Funding:** The research benefited however from the analytical platforms (SCMEM, LA-ICP-MS) at GeoRessources in Nancy, which are funded by the Labex Ressources 21 (ANR-10-LABX-21-RESSOURCES21), the Région Lorraine, and the European Community through the FEDER program.

**Data Availability Statement:** Data are available upon request from the authors.

**Acknowledgments:** The authors would like to thank P. Bavuz and the Club de Minéralogie de Chamonix for providing a part of the studied material; B. Poty, who initiated all the work carried out in Nancy on Mont Blanc; and Andrei Lecomte, Olivier Rouer, Marie-Camille Caumon, and Marie-Christine Boiron for their contribution to SEM, electron microprobe, and Raman analyses, respectively. Marie-Christine Boiron is warmly acknowledged for her proofreading. Three anonymous reviewers are thanked for their constructive comments. Mr Gillbert Li is warmly acknowledged for his kind invitation to submit this paper to Crystals.

**Conflicts of Interest:** The authors declare no conflicts of interest.

## Appendix A

**Table A1.** Chemical compositions with the structural formulas of analysed titanites.

Wt. %	Al <sub>2</sub> O <sub>3</sub>	SiO <sub>2</sub>	CaO	TiO <sub>2</sub>	Fe <sub>2</sub> O <sub>3</sub>	Y <sub>2</sub> O <sub>3</sub>	Nb <sub>2</sub> O <sub>3</sub>	ZrO <sub>2</sub>	F	Total
Périades	1.22	30.06	28.58	38.56	0.17	0.78	1.16	0.31	0.00	100.99
Périades	1.24	30.49	28.41	38.38	0.16	0.75	1.29	0.26	0.00	101.12
Périades	1.25	30.41	28.42	38.24	0.14	0.86	1.36	0.26	0.00	101.07
Périades	1.30	30.26	27.97	37.93	0.22	0.81	1.62	0.22	0.00	100.53
Périades	1.13	31.25	28.34	39.71	0.13	0.99	0.75	0.00	0.00	102.42
Périades	1.36	30.45	28.37	37.65	0.30	0.78	1.83	0.30	0.00	101.31
Périades	1.44	30.23	28.16	37.55	0.28	0.76	1.85	0.28	0.00	100.80
Périades	1.47	30.11	28.52	37.73	0.30	0.93	1.60	0.20	0.00	101.13
Périades	1.45	29.79	28.11	37.66	0.26	0.84	1.66	0.21	0.00	100.21
Périades	1.57	30.04	28.08	37.91	0.03	0.92	1.76	0.05	0.00	100.39
Périades	1.54	30.18	28.46	37.56	0.20	0.82	1.84	0.19	0.00	100.97
Périades	1.55	29.96	28.52	37.23	0.11	0.77	2.13	0.23	0.00	100.60
Périades	1.54	30.25	28.39	37.26	0.27	0.75	2.25	0.18	0.00	101.13
Périades	1.58	30.48	28.43	38.30	0.16	0.78	1.64	0.07	0.00	101.58
Périades	1.70	30.25	28.56	37.88	0.33	0.71	1.72	0.07	0.00	101.52
Périades	1.73	30.54	28.59	38.68	0.07	0.28	0.42	0.07	0.00	100.44
Périades	1.53	30.12	28.32	37.52	0.11	0.75	1.99	0.30	0.00	100.74
Périades	1.52	30.25	28.46	38.26	0.20	0.82	1.40	0.34	0.00	101.43
Périades	1.47	30.48	28.58	38.41	0.30	0.79	1.26	0.25	0.00	101.81
Périades	1.22	30.25	28.55	38.69	0.21	0.76	0.82	0.17	0.00	100.86
Courtes	2.84	30.47	29.51	37.35	0.73	0.00	0.00	0.00	0.49	102.05
Courtes	2.83	30.67	29.53	37.14	0.58	0.00	0.00	0.00	0.50	101.77
Courtes	3.25	30.73	29.39	36.59	0.61	0.00	0.08	0.01	0.62	101.83
Courtes	3.57	30.80	29.48	36.47	0.62	0.00	0.00	0.00	0.67	102.17
Courtes	3.38	30.58	29.62	36.81	0.60	0.00	0.04	0.05	0.53	102.15
Courtes	3.36	30.68	29.40	36.41	0.57	0.00	0.00	0.00	0.52	101.45
Courtes	3.32	30.26	29.15	36.44	0.66	0.00	0.01	0.07	0.55	101.05
Courtes	3.14	29.98	29.25	36.69	0.63	0.00	0.00	0.08	0.52	100.86
Courtes	3.07	30.86	29.65	37.20	0.44	0.00	0.00	0.00	0.54	102.16
Courtes	3.22	30.75	29.39	37.03	0.49	0.00	0.00	0.06	0.52	101.90
Courtes	3.48	31.05	29.22	35.94	0.76	0.00	0.00	0.00	1.23	102.36
Courtes	3.60	31.27	28.86	35.31	0.81	0.00	0.00	0.00	0.82	101.40
Courtes	3.17	31.11	29.13	36.45	0.48	0.00	0.00	0.00	0.84	101.61
Charlet Straton	4.04	30.06	26.21	29.67	0.00	0.00	0.00	0.00	0.00	89.98
Charlet Straton	2.96	25.58	27.32	33.89	0.00	0.00	0.00	0.00	0.00	89.75
Charlet Straton	5.50	33.89	24.63	31.05	0.00	0.00	0.00	0.00	0.00	95.07
Charlet Straton	5.91	30.96	31.10	32.02	0.00	0.00	0.00	0.00	0.00	99.99
Charlet Straton	3.49	28.85	30.51	37.15	0.00	0.00	0.00	0.00	0.00	100.00
Petites Jorasses	8.26	33.64	27.24	26.74	0.00	0.00	0.00	0.00	0.00	97.41

Table A1. Cont.

Wt. %	Al <sub>2</sub> O <sub>3</sub>	SiO <sub>2</sub>	CaO	TiO <sub>2</sub>	Fe <sub>2</sub> O <sub>3</sub>	Y <sub>2</sub> O <sub>3</sub>	Nb <sub>2</sub> O <sub>3</sub>	ZrO <sub>2</sub>	F	Total
Petites Jorasses	6.72	32.97	28.66	31.65	0.00	0.00	0.00	0.00	0.00	100.00
A. du Tour	7.66	33.53	29.44	29.37	0.00	0.00	0.00	0.00	0.00	100.00
A. du Tour	7.94	32.34	29.39	30.33	0.00	0.00	0.00	0.00	0.00	100.00
A. du Tour	7.75	33.32	30.46	28.48	0.00	0.00	0.00	0.00	0.00	100.01

## References

- McLeod, G.W.; Dempster, T.J.; Faithfull, J.W. Deciphering magma-mixing processes using zoned titanite from the Ross of Mull Granite, Scotland. *J. Petrol.* **2010**, *52*, 55–82. [CrossRef]
- John, T.; Klemm, R.; Klemme, S.; Pfänder, J.; Elis Hoffmann, J.; Gao, J. Nb–Ta fractionation by partial melting at the titanite–rutile transition. *Contrib. Mineral. Petrol.* **2011**, *161*, 35–45. [CrossRef]
- Bonamici, C.E.; Kozdon, R.; Ushikubo, T.; Valley, J.X. High-resolution P–T–t paths from  $\delta^{18}\text{O}$  zoning in titanite: A snapshot of late-orogenic collapse in the Grenville of New York. *Geology* **2011**, *39*, 959–962. [CrossRef]
- Kowallis, B.J.; Christiansen, E.H.; Dorais, M.J.; Winkel, A.; Henze, P.; Franzen, L.; Mosher, H. Variation of Fe, Al, and F Substitution in Titanite (Sphene). *Geosciences* **2022**, *12*, 229. [CrossRef]
- Jung, S.; Hellebrand, E. Textural, geochronological and chemical constraints on polygenetic titanite and monogenetic apatite from a mid-crustal shear zone: An integrated EPMA, SIMS, and TIMS study. *Chem. Geol.* **2007**, *241*, 88–107. [CrossRef]
- Laurent, O.; Zeh, A.; Gerdes, A.; Villaros, A.; Gros, K.; Slaby, E. How do granitoid magmas mix with each other? Insights from textures, trace elements and Sr–Nd isotopic composition of apatite and titanite from the Matok Pluton (South Africa). *Contrib. Mineral. Petrol.* **2017**, *172*, 80. [CrossRef]
- Henze, P.K.; Christiansen, E.H.; Kowallis, B.J.; Dorais, M.J.; Mosher, H.D.; Franzen, L.M.; Martin, A.J.; Nabelek, P.I. Titanite geochemistry and textures: Implications for magmatic and post-magmatic processes in the Notch Peak and Little Cottonwood granitic intrusions, Utah. *Am. Mineral.* **2022**, *108*, 226–248. [CrossRef]
- Bernau, V.R.; Franz, G. Crystal chemistry and genesis of Nb-, V-, and Al-rich metamorphic titanite from Egypt and Greece. *Can. Mineral.* **1987**, *25*, 695–705.
- Enami, M.; Suzuki, K.; Liou, J.G.; Bird, D.K. Al–Fe<sup>3+</sup> and F–OH substitutions in titanite and constraints on their P–T dependence. *Eur. J. Mineral.* **1993**, *5*, 219–231. [CrossRef]
- Hu, H.; Li, J.; McFarlane, C.R.M.; Nasdala, L.; Broska, I. Hydrothermal titanite from the Chengchao iron skarn deposit; temporal constraints on iron mineralization, and its potential as a reference material for titanite U–Pb dating. *Mineral. Petrol.* **2017**, *111*, 593–608. [CrossRef]
- Leloup, P.H.; Arnaud, N.; Sobel, E.R.; Lacassin, R. Alpine thermal and structural evolution of the highest external crystalline massif: The Mont Blanc. *Tectonics* **2005**, *24*, 4. [CrossRef]
- Fabre, C.; Boiron, M.-C.; Dubessy, J.; Cathelineau, M.; Banks, D.A. Paleo-fluid chemistry of a single fluid event: A bulk and in-situ multi-technique analysis (LIBS, Raman spectroscopy) of an Alpine fluid. *Chem. Geol.* **2002**, *182*, 249–264. [CrossRef]
- Rolland, Y.; Rossi, M. Two-stage fluid flow and element transfers in shear zones during collision burial–exhumation cycle: Insights from the Mont Blanc Crystalline Massif (Western Alps). *J. Geodyn.* **2016**, *101*, 88–108. [CrossRef]
- Rolland, Y.; Cox, S.; Boullier, A.-M.; Pennacchioni, G.; Mancktelow, N. Rare earth and trace element mobility in mid-crustal shear zones: Insights from the Mont Blanc Massif (Western Alps). *Earth Planet. Sci. Lett.* **2003**, *214*, 203–219. [CrossRef]
- Bussy, F.; Schaltegger, U.; Marro, C. The age of the Mont-Blanc granite (Western Alps): A heterogeneous system dated by Rb–Sr whole-rock determinations on its microgranular enclaves. *Schweiz. Mineral. Petrogr. Mitt.* **1989**, *69*, 3–313.
- Cenki-Tok, B.; Darling, J.; Rolland, Y.; Dhuime, B.; Storey, C. Direct dating of mid-crustal shear zones with synkinematic allanite: New in-situ U–Th–Pb geochronological approaches applied to the Mont Blanc massif. *Terra Nova* **2012**, *26*, 29–37. [CrossRef]
- Poty, B.; Stalder, H.A.; Weisbrod, A. Fluid inclusions studies in quartz from fissures of western and central Alps. *Schweiz. Mineral. Petrogr. Mitt.* **1974**, *54*, 717–752.
- Marshall, D.; Pfeifer, H.R.; Hunziker, J.C.; Kirschner, D. A pressure–temperature–time path for the NE Mont-Blanc massif: Fluid-inclusion: Isotopic and thermobarometric evidence. *Eur. J. Mineral.* **1998**, *10*, 1227–12240. [CrossRef]
- Cathelineau, M.; Ayt Ougougdal, M.; Banks, D.; Lespinasse, M.; Boiron, M.C.; Poty, B. Fluid inputs and mass transfer during Alpine brittle deformation of the Mont-Blanc granite. *Bol. Soc. Esp. Miner.* **1995**, *18*, 34–35.
- Poty, B.; Cathelineau, M. La formation des cristaux dans les fentes alpines du massif du Mont-Blanc. Règne Minéral, Hors Série V «Minéralogie du Massif du Mont Blanc. 1999, pp. 19–21. Available online: <https://www.minerauxetfossiles.com/produit/le-regne-mineral-hors-serie-1999-mineralogie-du-massif-du-mont-blanc-2/> (accessed on 18 April 2024).
- Hauy, R.J. Traité de minéralogie. In *Sphène*; Conseil des Mines, Louis imp.: Paris, France, 1801; Volume 3, pp. 114–119.

22. Lacroix, A. *Minéralogie de la France*. In *Particular Sphère*; Librairie Polytechnique, Baudry et Cie: Paris, France, 1896; Volume 2, pp. 233–254.
23. Patton, C.; Hellstrom, J.; Paul, B.; Woodhead, J.; Hergt, J. Iolite: Freeware for the visualisation and processing of mass spectrometric data. *J. Anal. At. Spectrom.* **2011**, *26*, 2508–2518. [[CrossRef](#)]
24. Longerich, H.P.; Jackson, S.E.; Günther, D. Inter-laboratory note. Laser ablation inductively coupled plasma mass spectrometric transient signal data acquisition and analyte concentration calculation. *J. Anal. At. Spectrom.* **1996**, *11*, 899–904. [[CrossRef](#)]
25. Oberti, R.; Smith, D.C.; Rossi, G.; Caucia, F. The crystal-chemistry of high-aluminium titanites. *Eur. J. Mineral.* **1991**, *3*, 777–792. [[CrossRef](#)]
26. Gu, J.; Xu, B.; Li, S.; Zhao, Y. Titanite Spectroscopy and In Situ LA-ICP-MS U–Pb Geochronology of Mogok, Myanmar. *Crystals* **2022**, *12*, 1050. [[CrossRef](#)]
27. Krüger, H.; Töbrens, D.M.; Tropper, P.; Haefeker, U.; Kahlenberg, V.; Fuchs, M.R.; Olieric, V.; Troitzsch, U. Single-crystal structure and Raman spectroscopy of synthetic titanite analog CaAlSiO<sub>4</sub>F. *Miner. Petrol.* **2015**, *109*, 631–641. [[CrossRef](#)]
28. Sahama, T.G. On the chemistry of the mineral titanite. *CR Soc. Geol. Finl.* **1946**, *19*, 88–120.
29. Frost, B.R.; Chamberlain, K.R.; Schumacher, J.C. Sphene (titanite): Phase relations and role as a geochronometer. *Chem. Geol.* **2000**, *172*, 131–148. [[CrossRef](#)]
30. Kohn, M.J. Titanite petrochronology—Chapter 13. In *Petrochronology: Methods and Applications*; Reviews in Mineralogy & Geochemistry; Kohn, M.J., Engi, M., Lanari, P., Eds.; Mineralogical Society of America: Chantilly, VA, USA, 2017; Volume 83, pp. 419–442.
31. Tiepolo, M.; Oberti, R.; Vannucci, R. Trace-element incorporation in titanite: Constraints from experimentally determined solid/liquid partition coefficients. *Chem. Geol.* **2002**, *191*, 105–119. [[CrossRef](#)]
32. Higgins, J.B.; Ribbe, P.H. The crystal chemistry and space groups of natural and synthetic titanites. *Am. Mineral.* **1976**, *61*, 878–888.
33. RRUFF Database. Available online: <https://rruff.info/titanite> (accessed on 15 November 2023).

**Disclaimer/Publisher’s Note:** The statements, opinions and data contained in all publications are solely those of the individual author(s) and contributor(s) and not of MDPI and/or the editor(s). MDPI and/or the editor(s) disclaim responsibility for any injury to people or property resulting from any ideas, methods, instructions or products referred to in the content.